J|A|C|S
ARTICLES

Published on Web 01/23/2009

Nanoparticles of Adaptive Supramolecular Networks Self-Assembled from Nucleotides and Lanthanide Ions

Ryuhei Nishiyabu,[†] Nozomi Hashimoto,[†] Ten Cho,[†] Kazuto Watanabe,[†] Takefumi Yasunaga,[‡] Ayataka Endo,[†] Kenji Kaneko,[§,||] Takuro Niidome,[†,||] Masaharu Murata,[⊥] Chihaya Adachi,[#] Yoshiki Katayama,[†,#] Makoto Hashizume,[‡] and Nobuo Kimizuka*[,†,||]

Department of Applied Chemistry, Graduate School of Engineering, Kyushu University, 744 Moto-oka Nishi-ku, Fukuoka 819-0395, Japan, Department of Advanced Medical Initiatives, Faculty of Medical Sciences, Kyushu University, 3-1-1 Maidashi, Higashi-ku Fukuoka 812-8582, Japan, Department of Materials Science and Engineering, Graduate School of Engineering, Kyushu University, 744 Moto-oka Nishi-ku, Fukuoka 819-0395, Japan, JST, CREST, Department of Nano-Biomedicine, Graduate School of Medical Sciences, Kyushu University, 3-1-1 Maidashi, Higashi-ku, Fukuoka 812-8582, Japan, and Center for Future Chemistry, Kyushu University, 744 Moto-oka, Nishi-ku, Fukuoka 819-0395, Japan

Received July 28, 2008; E-mail: n-kimi@mail.cstm.kyushu-u.ac.jp

Ⓦ **This paper contains enhanced objects available on the Internet at http://pubs.acs.org/jacs.**

Abstract: Amorphous nanoparticles of supramolecular coordination polymer networks are spontaneously self-assembled from nucleotides and lanthanide ions in water. They show intrinsic functions such as energy transfer from nucleobase to lanthanide ions and excellent performance as contrast enhancing agents for magnetic resonance imaging (MRI). Furthermore, adaptive inclusion properties are observed in the self-assembly process: functional materials such as fluorescent dyes, metal nanoparticles, and proteins are facilely encapsulated. Dyes in these nanoparticles fluoresce in high quantum yields with a single exponential decay, indicating that guest molecules are monomerically wrapped in the network. Gold nanoparticles and ferritin were also wrapped by the supramolecular shells. In addition, these nucleotide/lanthanide nanoparticles also serve as scaffolds for immobilizing enzymes. The adaptive nature of present supramolecular nanoparticles provides a versatile platform that can be utilized in a variety of applications ranging from material to biomedical sciences. As examples, biocompatibility and liver-directing characteristics in *in vivo* tissue localization experiments are demonstrated.

Introduction

The ability to encapsulate molecules and nanoscale materials in supramolecular networks holds promise to tailor and improve their functions for technologically important applications. The key feature to encapsulate guest molecules and nanomaterials is adaptability, which has been one of the unexplored functions in supramolecular chemistry.[1] The adaptive molecular networks most ubiquitous in nature are those of hydrogen bonding within the hydration shell, which are self-assembled on hydrophobic molecules by flexibly following their shapes.[2] They play important roles in determining conformation, dynamics, intermolecular interaction and function of the surrounded guest molecules. By replacing the roles of hydrogen-bonding shells with supramolecular networks, adaptive supramolecular shell would be obtained. Even a large variety of supramolecular host compounds have been developed so far,[3,4] they are only designed to accommodate small guest molecules. Moreover, these systems exclude adaptive inclusion properties at the cost of achieving specific molecular recognition. Current methods suffer from limitations in preparing huge supramolecular host molecules, which flexibly encapsulate large molecules and/or nanomaterials.

We describe herein nanoparticles (NPs) of adaptive supramolecular networks self-assembled in water from nucleotides and lanthanide ions (Figure 1a). Nucleotides are selected as components because they are biocompatible and show rich structural diversity with multiple functional groups—nucleobases and phosphate groups—which can serve as bidentate ligands. In contrast to nucleotide-sequence-directed hybridization in oligonucleotides,[5] the use of nucleotides as components for self-assembly has been largely limited to G-quartets formed by 5′-

[†] Department of Applied Chemistry.
[‡] Department of Advanced Medical Initiatives.
[§] Department of Materials Science and Engineering.
[||] JST, CREST.
[⊥] Department of Nano-Biomedicine.
[#] Center for Future Chemistry.

(1) Lehn, J.-M. *Proc. Natl. Acad. Sci. U.S.A.* **2002**, *99*, 4763–4768.
(2) Daidone, I.; Ulmschneider, M. B.; Nola, A. D.; Amadei, A.; Smith, J. C. *Proc. Natl. Acad. Sci. U.S.A.* **2007**, *104*, 15230–15235.
(3) Fujita, M.; Tominaga, M.; Hori, A.; Therrien, B. *Acc. Chem. Res.* **2005**, *38*, 369–378.
(4) Pluth, M. D.; Raymond, K. N. *Chem. Soc. Rev.* **2007**, *36*, 161–171.
(5) Feldkamp, U.; Niemeyer, C. M. *Angew. Chem., Int. Ed.* **2006**, *45*, 1856–1876.

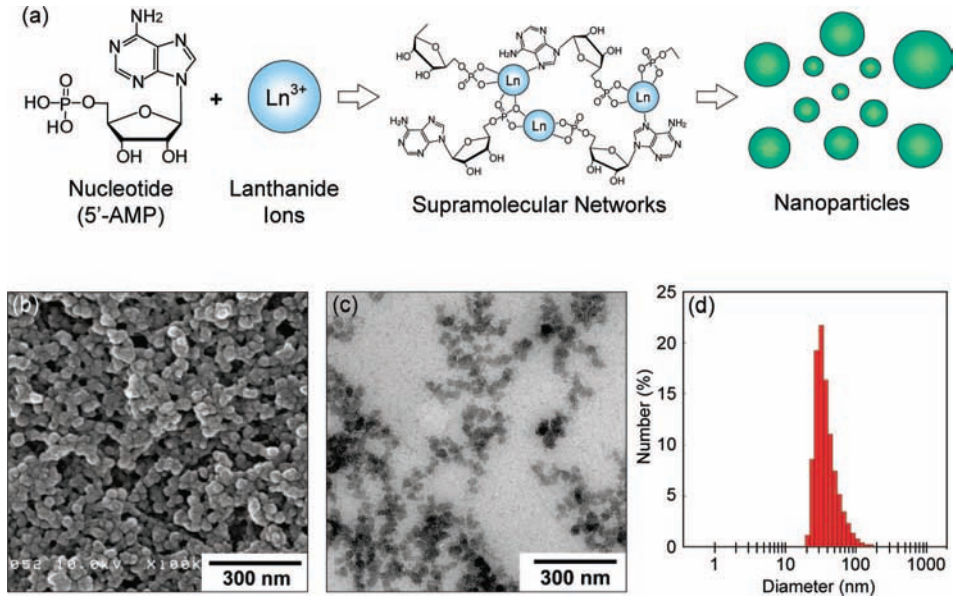

Figure 1. Nanoparticles formed by self-assembly of nucleotides and lanthanide ions. (a) A schematic illustration of nanoparticle formation through the self-assembly of 5′-AMP and Gd^{3+} ions. (b) SEM image of 5′-AMP/Gd^{3+} nanoparticles prepared in water. (c) TEM image of 5′-AMP/Gd^{3+} nanoparticles dispersed in aqueous poly(sodium 4-styrene sulfonate). (d) Size distribution histogram obtained by DLS measurement.

GMP and alkali metal ions[6]and their application to dynamic combinatorial libraries.[7] Meanwhile, we have recently reported that self-assembly of mononucleotide 5′-ATP, amino acids, and cationic cyanine dyes spontaneously give supramolecular nanofibers with excitonic chromophore interactions.[8,9] They showed that small biomolecules without self-assembling characteristics could serve as molecular building blocks, when they interacted with suitable counterparts. Lanthanide ions are selected as partners because they exhibit large coordination numbers and high coordination flexibility, which properties are suitable for making networks that flexibly adapt the size and shape of guest materials. Moreover, they display a wide variety of unique characteristics such as magnetic,[10] luminescent[11] and catalytic[12] properties. Though interactions between nucleotides, oligonucleotides and lanthanide ions have been reported,[13,14] there has been no report on nanostructures self-assembled from these components. We show that nucleotide/lanthanide nanoparticles display unique properties such as sensitized lanthanide luminescence and excellent performance as MRI contrast agents, depending on the combination of nucleotides and lanthanide ions. Importantly, they show adaptive inclusion properties for guest materials which range from molecules to nanomaterials, in the self-assembly process. As basic applications of these self-assembling nanoparticles, immobilization of enzymes, cellular uptake, biocompatibility and *in vivo* tissue localization are exemplified.

Results and Discussion

Self-Assembly of Nucleotides and Lanthanide Ions in Water. Spontaneous self-assembly of nucleotides and lanthanide ions was investigated prior to the presence of guest materials. Mixing of aqueous $GdCl_3$ (10 mM) with equimolar 5′-AMP in HEPES buffer (pH 7.4) resulted in colorless precipitates. These precipitates were washed with pure water several times and collected by centrifugation. These precipitates were redispersible in water, and formation of nanoparticles with diameters of 41 ± 5 nm was confirmed by scanning electron microscopy (SEM, Figure 1b). These 5′-AMP/Gd^{3+} nanoparticles were stably dispersed in aqueous polyelectrolytes such as poly(sodium 4-styrene sulfonate, PSS), as confirmed by transmission electron microscopy (TEM, Figure 1c). In dynamic light scattering (DLS) measurement, an average diameter of 40.7 ± 9.7 nm was observed (Figures 1d). This DLS-diameter is consistent with those observed in SEM and TEM micrographs. The stoichiometry of nanoparticles determined by precipitation titration experiments and SEM-energy dispersive X-ray spectroscopy was 5′-AMP:Gd^{3+} = 3:2 (Figures S1 and S2, Supporting Information). This molar ratio indicates that formation of nanoparticles is controlled by electrostatic interactions. The variation in concentration of initial solutions and their mixing rates did not cause significant changes in the morphology or size of nanoparticles (Figures S3 and S4, Supporting Information). Structural stability of nanoparticles is secured by polymeric coordination structures formed by nucleobases, phosphate groups and lanthanide ions, as confirmed by infrared absorption spectroscopy (Figure S5 and Table S1, Supporting Information). Powder X-ray diffraction analysis of nanoparticles showed that these supramolecular nanoparticles were amorphous (Figure S6, Supporting Information), as expected from asymmetric chemical structure of nucleotides and high coordination flexibility of lanthanide ions.

Formation of nanoparticles is widely observed for variety of nucleotide/lanthanide combinations (Figures S7−S8, Supporting Information, lanthanide ions; Sc^{3+}, Y^{3+}, La^{3+}, Ce^{3+}, Pr^{3+}, Nd^{3+}, Sm^{3+}, Eu^{3+}, Gd^{3+}, Tb^{3+}, Dy^{3+}, Ho^{3+}, Er^{3+}, Yb^{3+}, and Lu^{3+}), and their sizes were predominantly dependent on the chemical structure of nucleotides (type of nucleobases, position of

(6) Davis, J. T. *Angew. Chem., Int. Ed.* **2004**, *43*, 668–698.
(7) Sreenivasachary, N.; Lehn, J.-M. *Proc. Natl. Acad. Sci. U.S.A.* **2005**, *102*, 5938–5943.
(8) Morikawa, M.-A.; Yoshihara, M.; Endo, T.; Kimizuka, N. *J. Am. Chem. Soc.* **2005**, *127*, 1358–1359.
(9) Shiraki, T.; Morikawa, M.-A.; Kimizuka, N. *Angew. Chem., Int. Ed.* **2008**, *47*, 106–108.
(10) Benelli, C.; Gatteschi, D. *Chem. Rev.* **2002**, *102*, 2369–2387.
(11) Bünzli, J -C. G.; Piguet, C. *Chem. Soc. Rev.* **2005**, *34*, 1048–1077.
(12) Kobayashi, S.; Sugiura, M.; Kitagawa, H.; Lam, W. W.-L. *Chem. Rev.* **2002**, *102*, 2227–2302.
(13) Lippert, B. *Coord. Chem. Rev.* **2000**, *200−202*, 487–516.
(14) Fu, P. K.-L.; Turro, C. *J. Am. Chem. Soc.* **1998**, *121*, 1–7.

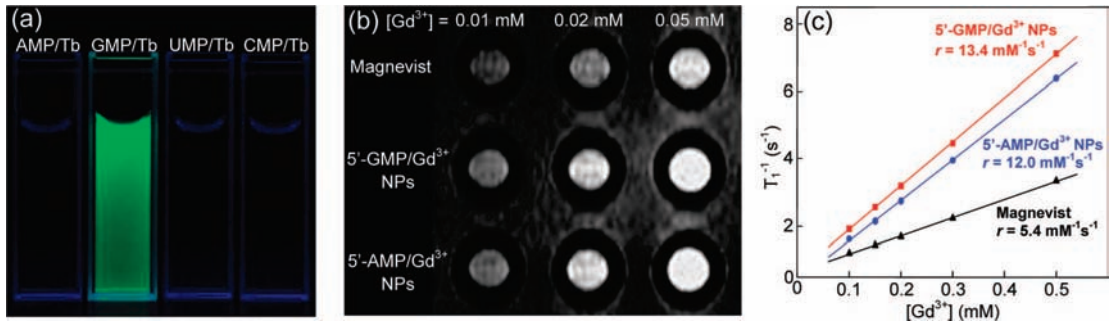

Figure 2. Luminescent and MR imaging abilities of nucleotide/lanthanide nanoparticles. (a) Photographs of aqueous dispersions of 5′-AMP/Tb^{3+}, 5′-GMP/Tb^{3+}, 5′-UMP/Tb^{3+}, and 5′-CMP/Tb^{3+} NPs ([nucleotide] = [Tb^{3+}] = 1×10^{-4} M, pH 7.4) under the UV light (254 nm). (b) T_1-weighted MR images of Magnevist, 5′-GMP/Gd^{3+} NPs and 5′-AMP/Gd^{3+} NPs in 0.1 M HEPES buffer containing 50 μg/mL of poly(sodium 4-styrene sulfonate) at pH 7.4. (c) Determination of longitudinal relaxivities (r_1) values for Magnevist, 5′-GMP/Gd^{3+} NPs and 5′-AMP/Gd^{3+} NPs.

phosphate groups, etc.). For example, complexation of Gd^{3+} ion with 5′-GMP, 3,5-cyclic GMP, and NAD^+ formed nanoparticles with diameters of 30 ± 5, 64 ± 10, and 179 ± 25 nm, respectively (Figure S9, Supporting Information). It is noteworthy that amorphous nanoparticles are formed instead of crystalline precipitates. It indicates rapid formation of nuclei and their self-assembly into nanoparticles, which are stable enough to keep their structural integrity (Figure S10 and S11, Supporting Information).

Intrinsic Functions of Nucleotide/Lanthanide Nanoparticles. The nucleotide/lanthanide nanoparticles show properties such as luminescence sensitized by energy transfer and performance as magnetic resonance imaging (MRI) contrast agents, which are enhanced by the self-assembly. When nanoparticles were self-assembled from 5′-AMP, 5′-GMP, 5′-UMP, or 5′-CMP and Tb^{3+} ions, intense green luminescence of Tb^{3+} was observed only for 5′-GMP/Tb^{3+}, with peaks at 492, 548, 588, 624, and 653 nm (Figures 2a and S12, Supporting Information). This is ascribed to energy transfer from guanine base to the emissive $^5D_4$ state of Tb^{3+} ion, which is promoted by coordination of O6 and N7 moieties to Tb^{3+} ions.[14] The luminescence quantum yield of 5′-GMP/Tb^{3+} nanoparticles in aqueous dispersion was determined to be 5%, while those of 5′-AMP/Tb^{3+}, 5′-UMP/Tb^{3+}, and 5′-CMP/Tb^{3+} nanoparticles were less than 1%. Luminescence of lanthanide ions are often quenched in water, due to deactivation of the excited states through O−H vibrational modes of coordinated water molecules.[11] Therefore, the observed intense emission of Tb^{3+} ions would reflect hydrophobic environment of the nanoparticle interior.

Chelates of paramagnetic Gd^{3+} ions have been used as magnetic resonance imaging (MRI) contrast agent, because of their effect to accelerate spin−lattice relaxation (T_1). The performance of nucleotide/Gd^{3+} nanoparticles as MRI contrast agent was investigated, since self-assembly of Gd^{3+} ions in nanoparticles is expected to increase the rotational correlation time τ_R, which would improve the relaxivity per Gd^{3+} ion.[15] Prior to the MRI measurement, leaching out of Gd^{3+} ions from 5′-AMP/Gd^{3+} and 5′-GMP/Gd^{3+} nanoparticles was examined by using thymolphthalein complexone as colorimetric indicator (Figure S13, Supporting Information). A very low concentration of free Gd^{3+} ions (ca. 6.5−8.6 μM) was estimated after keeping the HEPES buffer solutions for 1 week, indicating negligible leaking from the nanoparticles.

Figure 2b shows T_1-weighted images obtained for aqueous dispersions of 5′-AMP/Gd^{3+} nanoparticles and 5′-GMP/Gd^{3+} nanoparticles, which are compared with those obtained for commercially available contrast agent $[Gd(DTPA)(H_2O)]^{2-}$ (Magnevist™, DTPA: diethylenetriaminepentaacetic acid). Very interestingly, aqueous dispersions of nucleotide/Gd^{3+} nanoparticles showed higher contrast compared to the case of Magnevist. Longitudinal relaxivities (r_1) values determined for 5′-AMP/Gd^{3+} and 5′-GMP/Gd^{3+} nanoparticles were $r_1 = 12.0$ and 13.4 $mM^{-1}s^{-1}$ (at the magnetic field of 0.3 T, Figures 2c and S14, Supporting Information), respectively, which were more than twice larger than that observed for Magnevist ($r_1 = 5.4$ $mM^{-1}s^{-1}$ at 0.3 T). These data clearly indicate superior MRI property of the nucleotide/Gd^{3+} nanoparticles. It is also noticeable that smaller 5′-GMP/Gd^{3+} nanoparticles (average diameter, 30 nm, Figure S15 left, Supporting Information) show larger r_1 value compared to that observed for larger 5′-AMP/Gd^{3+} nanoparticles (average diameter, 41 nm, Figure S15 right, Supporting Information). The observed inverse size dependence of relaxivity indicates contribution of Gd^{3+} ions near at the surface, since those in the nanoparticle interior assume decrease in the water-exchange lifetime due to restricted mobility of water molecules.[16,17]

Adaptive Inclusion of Guest Materials in the Self-Assembly Process. Very interestingly, the supramolecular networks of nucleotide/lanthanide show adaptive inclusion properties in their self-assembly process. Water soluble dyes (**1**−**8**, Figure 3a) were employed as guest molecules to evaluate inclusion properties of nucleotide/lanthanide networks. HEPES buffer solutions of dyes and nucleotides were mixed with aqueous $GdCl_3$, and the resulting suspensions were ultracentrifuged to precipitate nanoparticles (Figure S16, Supporting Information). Spectroscopic investigation of the supernatants showed effective incorporation of anionic dyes into nanoparticles, whereas most of cationic dyes were left in the supernatants (Figure 3b). The efficient binding of anionic dyes implies coordination of their carboxyl groups to Gd^{3+} ions. Confocal laser scanning microscopy (CLSM) was conducted for dye **2**-doped NADH/La^{3+} microspheres, showing that the dyes were located inside (Figures 3c and S17). Interestingly, the dye-doped 5′-AMP/Lu^{3+} nanoparticles showed intense luminescence even in the solid state (Figures 3d right and S18, Supporting Information. Absolute quantum yields Φ_{PL}: dye **1** in NPs, 49%, dye **2** in NPs; 29%, dye **3** in NPs, 24%). This is surprising because these solid dyes

(15) Raymond, K. N.; Pierre, V. C. *Bioconjugate Chem.* **2005**, *16*, 3–8.
(16) Rieter, W. J.; Taylor, K. M. L.; An, H.; Lin, W.; Lin, W. *J. Am. Chem. Soc.* **2006**, *128*, 9024–9025.
(17) Bridot, J.-L.; Faure, A.-C.; Laurent, S.; Riviére, C.; Billotey, C.; Hiba, B.; Janier, M.; Josserand, V.; Coll, J.-L.; Elst, L. V.; Muller, R.; Roux, S.; Perriat, P.; Tillement, O. *J. Am. Chem. Soc.* **2007**, *129*, 5076–5084.

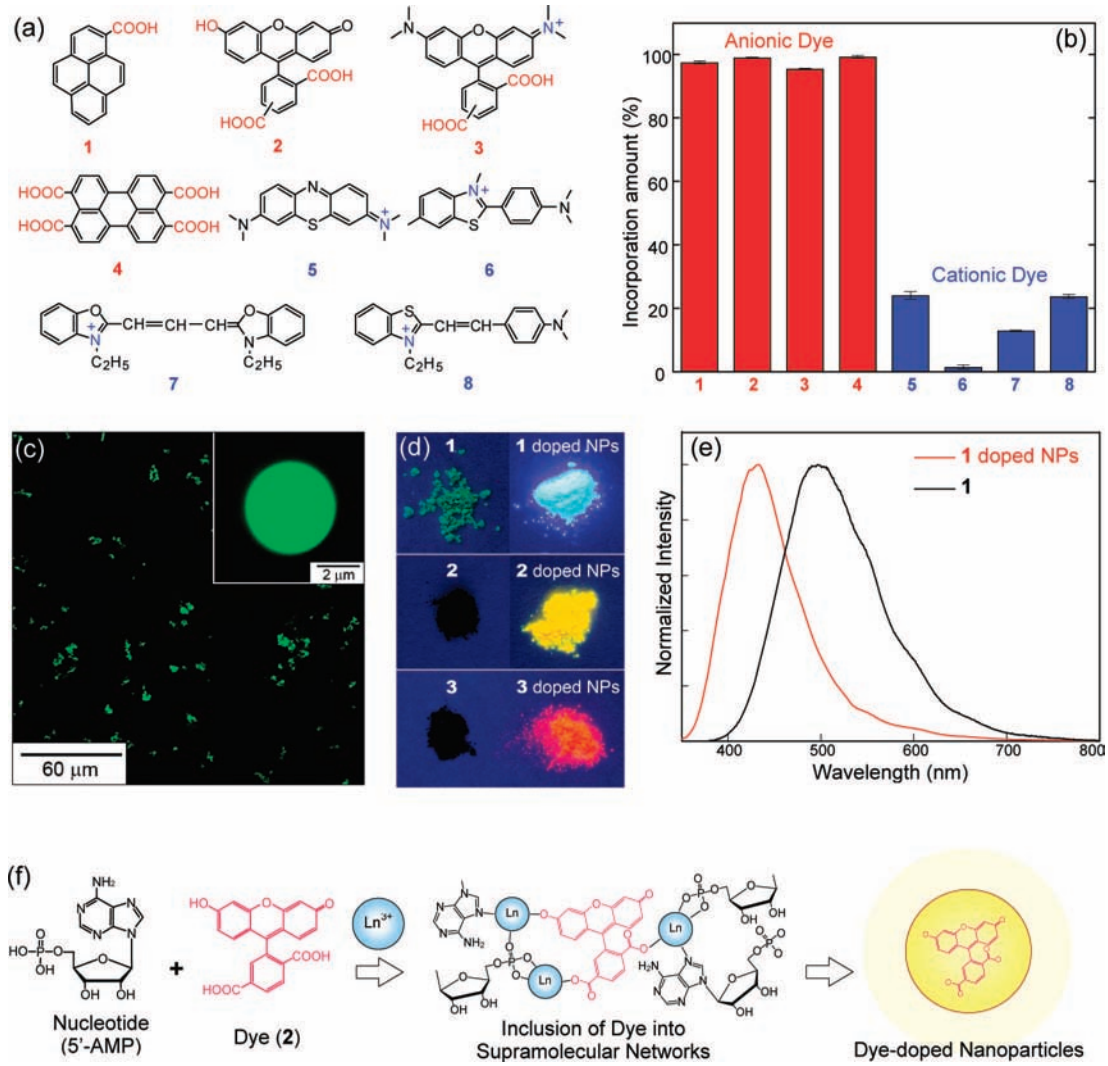

Figure 3. Incorporation of dyes into nanoparticles of nucleotide/lanthanide supramolecular networks. (a) Chemical structures of guest dyes. (b) Binding ratio (%) of various dyes to 5′-AMP/Gd^{3+} NPs. (c) CLSM image of **2**-doped NADH/La^{3+} microspheres dispersed in water. (d) Photographs of powder samples of solid dyes **1**, **2**, and **3** (left) and **1**, **2**, and **3**-doped 5′-AMP/Lu^{3+} nanoparticles (right). Samples were illuminated by the 365 nm UV light. (e) Luminescent spectra of powdery samples of **1**-doped 5′-AMP/Lu^{3+} nanoparticles (red line) and **1** (black line). Samples were excited at 350 nm. (f) Schematic illustration of adaptive dye encapsulation in supramolecular networks. Nanoparticles were prepared by adding aqueous lanthanide ions to the mixtures of nucleotide and dyes dissolved in HEPES buffer.

give very weak fluorescences ($\Phi_{PL} \approx 1\%$), due to overwhelming nonradiative deactivation of excited states governed by nonfluorescent aggregates acting as energy traps (Figure 3d, left). The dye **1** incorporated in nanoparticles showed luminescence at $\lambda_{max} = 432$ nm with a single luminescence lifetime of $\tau_{PL} = 7.0$ ns (Figures 3e and S19 left, Supporting Information). On the other hand, dye **1** in the powdery state showed very weak red-shifted fluorescence ($\lambda_{max} = 497$ nm) with multicomponent decay (Figures 3e and S19 right, Supporting Information). The single-component decay observed for the fluorescence of dye-doped nanoparticles indicates that dyes were isolated in supramolecular shells without aggregation. It reflects that growing supramolecular networks bind and accommodate anionic dyes by flexibly adapting to the shape of guest molecules (Figure 3f). This adaptive inclusion process would be ascribed to the high coordination flexibility of lanthanide ions and amorphous structure of supramolecular networks, which prevented segregation of the guest molecules.

The adaptive inclusion ability of nucleotide/lanthanide nanoparticles is also applicable to nanosized guests such as gold nanoparticles (AuNPs). AuNPs capped by 5′-GMP molecules[18,19] (Figure S20, Supporting Information) in HEPES buffer was mixed with aqueous $GdCl_3$. Purple precipitates were immediately formed, which were redispersible in water by ultrasonication. TEM and high-resolution TEM (HR-TEM) observation of the redispersed sample clearly showed that AuNPs were surrounded by the amorphous shell of supramolecular networks (Figure 4a and b). This nature was further supported by a three-dimensional reconstructed volume obtained by the combination of transmission electron microscopy (TEM-CT) and computed tomography (see video showing a 3D view of the gold nanoparticles-wrapped nanoparticles obtained by electron tomography), in which gold nanoparticles were intentionally colored in gold and 5′-GMP/Gd^{3+} network were in greenish blue. In addition, the presense of peaks assigned to Au, Gd, and P were confirmed by the coexistence of peaks assigned to Au, Gd, and P in the EDX microanalysis (Figure S20, Supporting Information). Surface plasmon resonance peak of

(18) Xie, J.; Lee, J. Y.; Wang, D. I. C. *Chem. Mater.* **2007**, *19*, 2823–2830.
(19) Zhao, W.; Gonzaga, F.; Li, Y.; Brook, M. A. *Adv. Mater.* **2007**, *19*, 1766–1771.

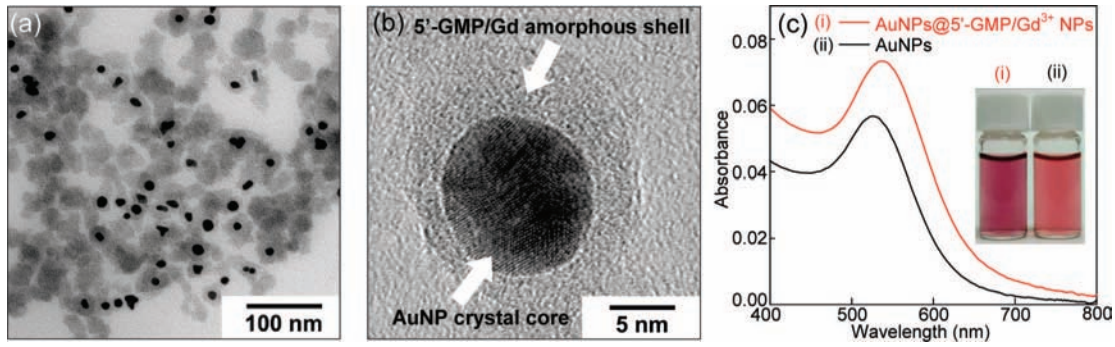

Figure 4. Inclusion of gold nanoparticles (AuNPs) in nucleotide/lanthanide nanoparticles. (a) TEM image of AuNPs encapsulated by the amorphous supramolecular shells of 5′-GMP/Gd^{3+} in aqueous dextran. (b) HR-TEM image of a AuNP wrapped by the supramolecular shell of 5′-GMP/Gd^{3+}. (c) Absorption spectra and photographs (inlet) of aqueous dispersions of AuNPs-wrapped 5′-GMP/Gd^{3+} NPs (AuNPs@5′-GMP/Gd^{3+} NPs) and as-prepared 5′-GMP-capped AuNPs. Nanoparticles were prepared by adding aqueous lanthanide ions to 5′-GMP and 5′-GMP-capped AuNPs dissolved in HEPES buffer ([dextran] = 10 mg/mL).

AuNPs encapsulated in 5′-GMP/Gd^{3+} nanoparticles was observed at 538 nm (Figure 4c(i)), which is red-shifted by 12 nm compared to that of the AuNPs formed in 5′-GMP/HEPES buffer (Figure 4c(ii), λ_{max} 526 nm). The observed shift is consistent with changes in the local environment of AuNPs surfaces caused by the wrapping by molecular networks of 5′-GMP/Gd^{3+}.[20]

The successful encapsulation of AuNPs in supramolecular networks prompted us further to investigate binding of proteins. Nanoparticles were prepared by adding aqueous $GdCl_3$ to mixtures of 5′-AMP and proteins dissolved in HEPES buffer (Figures S21 and S22, Supporting Information). Ferritin (pI = 4.5) and fluorophore (Alexa 488)-labeled proteins (bovine serum albumin (BSA, pI = 4.7), peanut agglutinin (PNA, pI = 5.7−6.7), concanavalin A (Con A, pI = 7.1), histone H1 (Histone, pI = 10.4)) were employed. In Figure 5a, binding ratio (%) of these biopolymers to 5′-AMP/Gd^{3+} nanoparticles as determined by the absorption intensity of supernatants are compared. Consistent with the dye-incorporation data (Figure 3b), anionic proteins (Ferritin, BSA, PNA, ConA) were effectively bound to nanoparticles, whereas cationic Histone showed lower affinity. The observed higher affinity of anionic proteins would be attributed to coordination of their carboxylate groups to Gd^{3+} ions in the networks.

The contact between anionic proteins and nucleotide/lanthanide networks was further confirmed by fluorescence resonance energy transfer (FRET). Nucleotide/lanthanide nanoparticles were prepared from 1,N^6-ethenoadenosine-labeled nucleotide (5′-ϵAMP) and Gd^{3+} ion in the presence of fluorophore Alexa 488-labeld BSA (Alexa-BSA). The chromophores of 5′-ϵAMP and Alexa 488 were employed as donor and acceptor, respectively (Figure S23, Supporting Information). Figure 5b displays fluorescence spectra of ternary Alexa-488 labeled BSA (Alexa-BSA)-incorporated 5′-ϵAMP/Gd^{3+} NPs (red, Alexa-BSA/ϵAMP/Gd^{3+} NPs). Spectra in blue broken lines represent the sum of two spectra obtained for Alexa-BSA/AMP/Gd^{3+} NPs and 5′-ϵAMP/Gd^{3+} NPs. The shoulder component at 520−540 nm in broken blue line is ascribed to the fluorescence of Alexa-BSA on 5′-AMP/Gd^{3+} nanoparticles excited directly by the 320-nm light. In Alexa-BSA/ϵAMP/Gd^{3+} NPs, quenching of 5′-ϵAMP fluorescence at 420 nm was observed (the red line in Figures 5b, S23). It was accompanied by the increase in fluorescence intensity of Alexa-488 (at 520 nm), indicating that energy transfer occurred from 5′-ϵAMP/Gd^{3+} to Alexa-488 on BSA. The observation of FRET from ϵAMP to Alexa 488 indicates that Alexa 488-labeled BSA is in well contact with the coordination networks formed by ϵAMP and Gd^{3+} ions.

Protein binding to nucleotide/lanthanide nanoparticles was visualized for ferritin, an iron-storage anionic protein containing iron oxide nanoparticle in its cavity. TEM observation conducted for the ternary mixture of ferritin, 5′-AMP and $GdCl_3$ showed iron oxide nanoparticles of ferritin bound to 5′-AMP/Gd^{3+} nanoparticles (Figure 5d). To further analyze the location of ferritins within 5′-AMP/Gd^{3+} nanoparticles, three-dimensional electron tomography using a scanning TEM with a high-angle annular dark-field (STEM-HAADF) method[21] was conducted. Very interestingly, the entire volume of ferritin were wrapped by the 5′-AMP/Gd^{3+} suprmolecular networks as confirmed by the STEM-HAADF images observed at 0° and tilted angle of ca. 70° (Figure S24, Supporting Information).

The binding of proteins to supramolecular nucleotide/lanthanide networks provides a new approach in the protein immobilization.[22−24] To introduce enzymatic activity, enzyme-immobilized 5′-CMP/Eu^{3+} nanoparticles were prepared by the following procedure. Aqueous $EuCl_3$ was added to the mixture of glucose oxidase (GOx, pI = 4.2), horse radish peroxidase (HRP, pI = 7.2) and 5′-CMP in HEPES buffer. The enzyme-co-immobilized 5′-CMP/Eu^{3+} nanoparticles obtained were accumulated on membrane filters and their enzymatic activity was investigated by using colorimetric enzyme-linked assay (Trinder reagent).[25] When colorless aqueous mixtures of glucose and Trinder reagent were dropped on these nanoparticles, the color immediately turned to violet (Figures 5e and S25, Supporting Information). On the other hand, there was no change in color for aqueous mixtures containing nonsubstrates for GOx; D-galactose, D-mannose, D-fructose or D-xylose. These observations clearly indicate that immobilized HRP and GOx maintained their enzymatic activities on 5′-CMP/Eu^{3+} networks.

Cellular uptake, Cytotoxicity, and Tissue Localization *in vivo*. The stability and adaptive inclusion properties of self-assembling nucleotide/lanthanide nanoparticles would be useful

(20) Ghosh, S. K.; Pal, T. *Chem. Rev.* **2007**, *107*, 4797–4862.
(21) Kaneko, K.; Inoke, K.; Freitag, B.; Hungria, A. B.; Midgley, P. A.; Hansen, T. W.; Zhang, J.; Ohara, S.; Adschiri, T. *Nano Lett.* **2007**, *7*, 421–425.
(22) Niemeyer, C. M. *Angew. Chem., Int. Ed.* **2001**, *40*, 4128–4158.
(23) Patil, A. J.; Muthusamy, E.; Mann, S. *Angew. Chem., Int. Ed.* **2004**, *43*, 4928–4933.
(24) Sokolova, V.; Epple, M. *Angew. Chem., Int. Ed.* **2008**, *47*, 1382–1395.
(25) Tamaoku, K.; Murao, Y.; Akiura, K.; Ohkura, Y. *Anal. Chim. Acta* **1982**, *136*, 121–127.

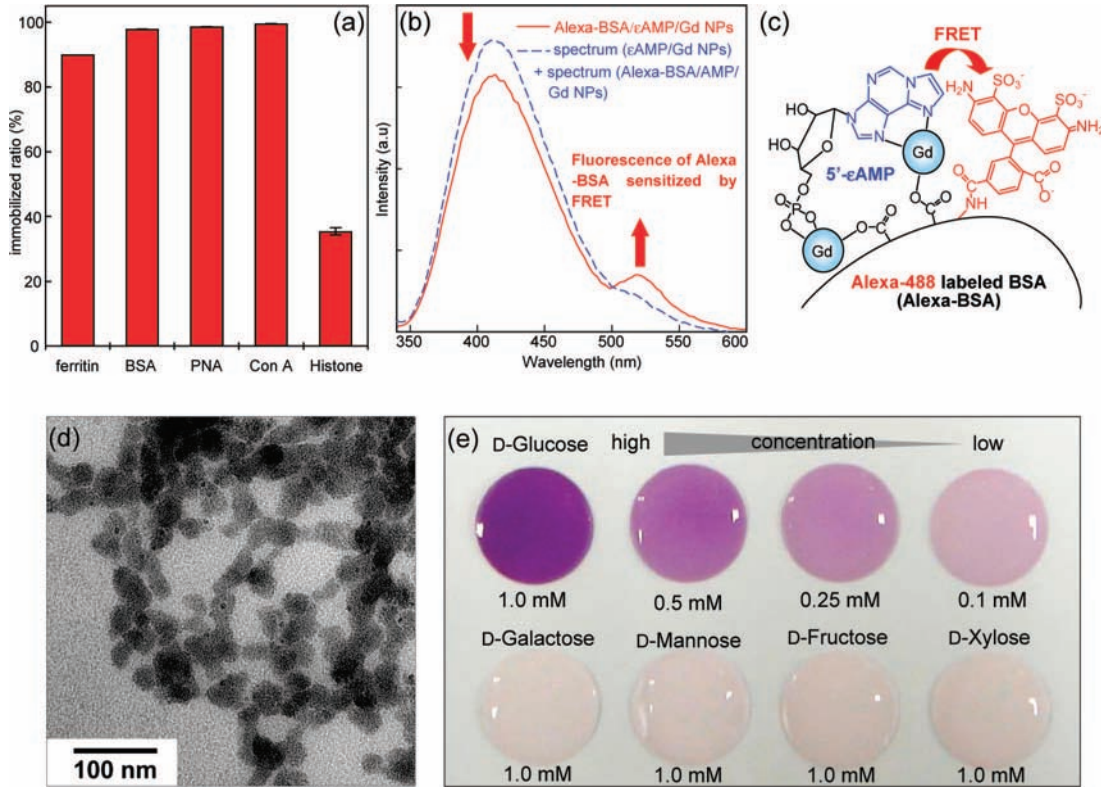

Figure 5. Immobilization of biomacromolecules to nucleotide/lanthanide nanoparticles. (a) Immobilized ratio (%) of ferritin, bovine serum albumin (BSA), peanut agglutinin (PNA), concanavalin A (Con A), and histone H1 (Histone) to 5′-AMP/Gd^{3+} NPs. Fluorophore-labeled proteins (except for ferritin) were used to quantitatively determine the binding ratio. (b) Fluorescence spectra of Alexa-488 labeled BSA (Alexa-BSA)-incorporated ϵAMP/Gd^{3+} NPs (Alexa-BSA/ϵAMP/Gd^{3+} NPs). Spectra in blue broken lines represent the sum of two spectra obtained for Alexa-BSA/AMP/Gd^{3+} NPs and for ϵAMP/Gd^{3+} NPs. Condition: [nucleotide] = [$GdCl_3$] = 5×10^{-4} M, 10 μg/mL Alexa-BSA in 5 mM HEPES buffer, λ_{ex}=320 nm. (c) Schematic illustration showing FRET from ϵAMP to Alexa 488-labeled BSA in the coordination networks. (d) TEM images of ferritin bound to 5′-AMP/Gd^{3+} NPs. Dots in high contrast (diameter, ca. 8nm) are iron oxide cores of ferritin. (e) Coupled enzyme activity test for horseradish peroxidase (HPR) and glucose oxidase (GOx)-immobilized 5′-CMP/Eu^{3+} NPs. Various monosaccharide solutions containing colorimetric reagent for peroxidase activity assay were placed on the HPR and GOx-immobilizaed 5′-CMP/Eu^{3+} NPs which were collected on membrane filters. The first row from the left to right: [D-glucose] = 1.0, 0.5, 0.25, 0.1 mM. The second row from the left to right: [D-galactose] = 1.0 mM, [D-mannose] = 1.0 mM, [D-fructose] = 1.0 mM, [D-xylose] = 1.0 mM containing 10 mM colorimetric reagent in 0.1 M HEPES buffer (pH 7.4).

in many disciplines, including the biological applications[26−29] as described below. Here, cellular uptake, biocompatibility and *in vivo* tissue localization were investigated to understand their basic properties.

Fluorescence dye **4** was intentionally doped as guest molecule to 5′-AMP/Gd^{3+} nanoparticles, in order to monitor their localization in cells and tissues by fluorescent microscopy (The absorption and fluorescence peak maxima of dye **4** in nanoparticles; 477 and 500 nm, respectively). The dye **4**-doped 5′-AMP/Gd^{3+} nanoparticles were dispersed in 0.1 M HEPES buffer (pH 7.4) containing chondroitin sulfate C, and were added to HeLa cells in Dulbecco's modified Eagle's medium containing 10%(v/v) heat-inactivated fetal bovine serum and 1% (v/v) antibiotics (DMEM+FBS). Fluorescence microscopy indicated uptake of dye **4**-doped 5′-AMP/Gd^{3+} nanoparticles into HeLa cells (Figures 6a and S26, Supporting Information), while dye **4** (Na^+ salt) alone was not internalized into these cells due to electrostatic repulsion between anionic dye molecule **4** and cell membranes. Colocalization of dye **4**-doped 5′-AMP/Gd^{3+} nanoparticles and LysoTracker Red, which is a hydrophobic fluorescence probe used to determine the location of lysosomes within cells, confirmed that the dye **4**-doped 5′-AMP/Gd^{3+} nanoparticles were localized to lysosomes, and not on the surfaces of the cells (Figures S26, Supporting Information). Nanoparticles showed negligible cytotoxicity as investigated by cell viability assay (Figure S27, Supporting Information), and high cell viability was observed for these cells in the presence of 5′-AMP/Gd^{3+} nanoparticles.

These observations lead us to study tissue localization of dye **4**-doped 5′-AMP/Gd^{3+} nanoparticles *in vivo*. The disposition of nanoparticles in mice was studied by fluorescence reflectance imaging (Figure 6b) and inductively coupled plasma mass spectroscopy (ICP-MS, Figure 6c). The fluorescence is observed only form the liver, which is consistent with the ICP-MS analysis for Gd^{3+} ions. These observations clearly indicate that dye **4**-doped 5′-AMP/Gd^{3+} nanoparticles were rapidly accumulated in the liver, presumably due to recognition of nanoparticles by hepatic reticuloendothelial system.[30] Liver toxicity of 5′-AMP/Gd^{3+} nanoparticles was also examined by enzymatic assay for aspartate aminotransferase (AST) and alanine aminotransferase (ALT) in the blood (Figure S28, Supporting Information). These data showed negligible effect in the levels of AST and ALT activity, indicating that 5′-AMP/Gd^{3+} nanoparticles are nontoxic to liver. These results clearly demonstrate the potential of dye-doped nucleotide/lanthanide nanoparticles for biological applications, especially as imaging agents for liver. On the other hand, the observed rapid clearance

(26) Pellegrino, T.; Kudera, S.; Liedl, T.; Javier, A. M.; Manna, L.; Parak, W. J. *Small* **2005**, *1*, 48–63.
(27) Ferrari, M. *Nat. Rev. Cancer* **2005**, *5*, 161–171.
(28) Gil, P. R.; Parak, W. J. *ACS Nano* **2008**, *11*, 2200–2205.
(29) Cheon, J.; Lee, J.-H. *Acc. Chem. Res.* **2008**, *41*, 1630–1640.

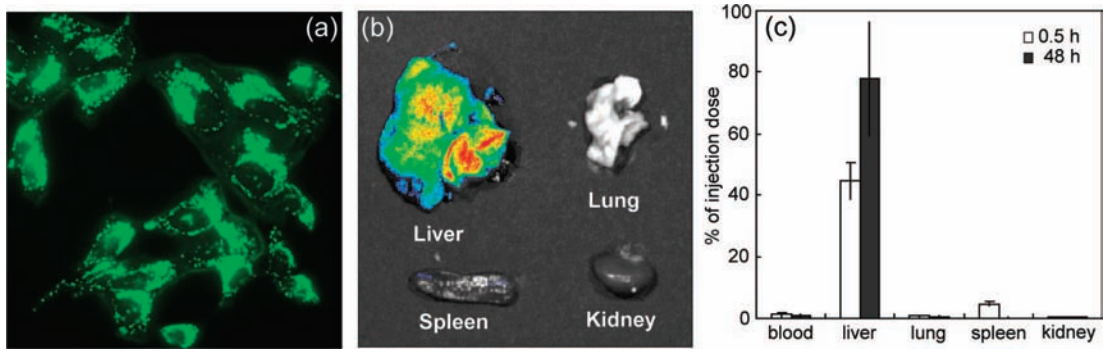

Figure 6. (a) Fluorescence microscopy of dye **4**-doped 5′-AMP/Gd^{3+} NPs added to HeLa cells. (b) Fluorescent images of tissue samples (live, spleen, kidney and lung) isolated from dye **4**-doped 5′-AMP/Gd^{3+} NPs-injected mice. (c) ICP-MS analysis of gadolinium in various isolated organs from mice, after 0.5 and 48 h of injection. 5′-AMP/Gd^{3+} NPs dispersed in 0.1 M HEPES buffer (pH 7.4) containing chondroitin sulfate C (10 mg/mL) was employed as a stock solution.

of 5′-AMP/Gd^{3+} nanoparticles from blood is undesirable for *in vivo* bioimaging of other tissues. This could be overcome by modification of nanoparticle surfaces by biologically inert PEG chains.[31−33] Surface functionalization of nucleotide/lanthanide nanoparticles is currently in progress in these laboratories and will be reported elsewhere.

Conclusions

In summary, we have demonstrated the spontaneous formation of nanoparticles of adaptive supramolecular networks self-assembled from nucleotides and lanthanide ions. These supramolecular networks display adaptive inclusion ability toward anionic molecules, nanoscale materials and also act as scaffolds for immobilizing enzymes. Moreover, they exhibit enhanced intrinsic functions such as nucleobase to lanthanide energy transfer, MR imaging properties. Adsorption of polyelectrolytes on nanoparticles surfaces improves their water solubility, and these nanoparticles show satisfactory biocompatibility. These features provide a simple way to design multifunctional nanomaterials. Although recently nucleotide capped inorganic nanoparticles[19,34] and amorphous coordination polymer nanoparticles[35−42] have been reported, adaptive inclusion properties as demonstrated in the present study have been unprecedented. We envisage that the concept of adaptive supramolecular nanonetworks will be extended to varied molecular self-assembling systems and they would find a broad range of applications from materials to biomedical sciences.

Experimental Section

Materials. Perylene-3,4,9,10-tetracarboxylic acid (dye **4**) was prepared according to reported procedure.[43] All the other chemicals and materials were purchased and used as received. Water was purified with a Direct-Q system (Millipore Co.).

Measurements. Scanning electron microscopy (SEM) and transmission electron microscopy (TEM) were performed by Hitachi S-5000 (acceleration voltage, 10 kV) and JEOL JEM-2010 (acceleration voltage, 120 kV), respectively. High-resolution TEM and energy dispersive X-ray microanalysis were performed on a Tecnai 20 (acceleration voltage, 200 kV). TEM-CT observations were conducted using a scanning TEM with a high-angle annular dark-field (STEM-HAADF) detector operated at 200 kV (Tecnai-F20) by achieving tilted series from −70 to +70°. For SEM measurements, nucleotide/lanthanide nanoparticles were collected on a membrane filter by filtration and the obtained membrane filter was dried in vacuum. The sample was coated with Pt on a HITACHI E-1030 ion sputter. For TEM measurement, nucleotide/lanthanide nanoparticle dispersion was put on carbon-meshed copper grid. After 30 s, the excess dispersion was removed by using a filtration paper and the resultant grid was dried in vacuum. The grid was measured without staining. Dynamic light scattering (DLS) for determination of nucleotide/lanthanide particle size was measured using the Malvern Zeta sizer Nano-ZS. Energy dispersive X-ray analysis (EDX) for bulk solid samples was carried out by Genesis 2000 X-ray Microanalysis System (EDAX) equipped with SEM Superscan SS-550 (SHIMADZU). Infrared spectra were obtained on a JASCO FTIR 460 Plus spectrometer. Powder X-ray diffraction (XRD) data were collected by Rigaku Multiflex X-ray diffractometer with Cu Kα radiation. MR images were obtained by using Hitachi Medico MRI AIRIS-II at 0.3 T. UV−vis absorption and emission spectra for solution samples were recorded on a JASCO V-550 and HITACHI F-4500 spectrophotometer, respectively and 1 mm and 1 cm cells were used. Confocal laser scanning microscopy (CLSM) was conducted with Carl Zeiss LSM510 instruments with a 63x oil-immersion objective. Luminescence spectra for solid samples were measured using multichannel photodetector system MCPD-7000 unit (Otsuka Electronic Co., Ltd.) equipped with a 500 W Xe arc lamp (Ushio, SX-UI500XQ) and a grating monochromator (JASCO, CT-10). Absolute photoluminescence quantum yields were determined by Absolute PL Quantum Yield Measurement System (HAMAMATSU, C9920−02). Luminescence decay curves were obtained by a streak camera

(30) Naito, M.; Hasegawa, G.; Ebe, Y.; Yamamoto, T. *Med. Electron Microsc.* **2004**, *37*, 16–28.
(31) Lee, H.; Lee, E.; Kim, D. K.; Jang, N. K.; Jeong, Y. Y.; Jon, S. *J. Am. Chem. Soc.* **2006**, *128*, 7383–7389.
(32) Ballou, B.; Lagerholm, B. C.; Ernst, L. A.; Bruchez, M. P.; Waggoner, A. S. *Bioconjugate Chem.* **2004**, *15*, 79–86.
(33) Kim, D.; Park, S.; Lee, J. H.; Jeong, Y. Y.; Jon, S. *J. Am. Chem. Soc.* **2007**, *129*, 7661–7665.
(34) Hinds, S.; Taft, J.; Levina, L.; Sukhovatkin, V.; Dooley, C. J.; Roy, M. D.; MacNeil, D. D.; Sargent, E. H; Kelley, S. O. *J. Am. Chem. Soc.* **2006**, *128*, 64–65.
(35) Oh, M.; Mirkin, C. A. *Nature* **2005**, *438*, 651–654.
(36) Sun, X.; Dong, S.; Wang, E. *J. Am. Chem. Soc.* **2005**, *127*, 13102–13103.
(37) Park, K. H.; Jang, K.; Son, S. U.; Sweigart, D. A. *J. Am. Chem. Soc.* **2006**, *128*, 8740–8741.
(38) Maeda, H.; Hasegawa, M.; Hashimoto, T.; Kakimoto, T.; Nishio, S.; Nakanishi, T. *J. Am. Chem. Soc.* **2006**, *128*, 10024–10025.
(39) Imaz, I.; Maspoch, D.; Rodriguez-Blanco, C.; Perez-Falcon, J. M.; Campo, J.; Ruiz-Molina, D *Angew. Chem., Int. Ed.* **2008**, *47*, 1857–1860.
(40) Jeon, Y-M.; Armatas, G. S.; Heo, J.; Kanatzidis, M. G.; Mirkin, C. A. *Adv. Mater.* **2008**, *20*, 2105–2110.
(41) Rieter, W. J.; Pott, K. M.; Taylor, K. M. L.; Lin, W. *J. Am. Chem. Soc.* **2008**, *130*, 11584–11585.
(42) Lin, W.; Rieter, W. J.; Taylor, K. M. L. *Angew. Chem., Int. Ed.* **2008**, .
(43) Takahashi, M.; Suzuki, Y.; Ichihashi, Y.; Yamashita, M.; Kawai, H. *Tetrahedron Lett.* **2006**, *48*, 357–359.

(Hamamatsu C4334) with a nitrogen gas laser ($\lambda = 337$ nm, pulse width ≈ 300 ps, and repetition rate = 20 Hz) as an excitation source. Fluorescent microscopy for biological assay was conducted with fluorescent microscopy (BIOREVO BZ-9000, KYENCE) equipped with PlanApo 60xH (Nikon) objective lens. UV−vis absorption determination for cell viability assay was performed by 96-well microplate reader (WALLAC 1420 Multilabel Counter, Perkin-Elmer). *In vivo* fluorescent imaging was performed by IVIS Lumina Imaging System (Xenogen).

Preparation of Nucleotide/Lanthanide Nanoparticles. The preparation of nucleotide/lanthanide nanoparticles was typically conducted as follows. To an aqueous solution of 10 mM 5′-AMP disodium salt in 0.1 M HEPES (2-[4-(hydroxyethyl)-1-piperazinyl]ethanesulfonic acid) buffer (1 mL, pH 7.4), was added aqueous 10 mM solution of $GdCl_3$ (1 mL) at room temperature. After 2 h, precipitates formed were collected by centrifugation (15000 rpm × 5 min). The obtained material was washed with pure water (2 mL) and collected by centrifugation (15000 rpm × 5 min). The washing procedure (water, 2 mL-centrifugation 15000 rpm × 5 min) was repeated once again. For SEM measurements, 5′-AMP/Gd^{3+} nanoparticles were collected on membrane filter. To enhance the dispersibility of nucleotide/lanthanide nanoparticles in water, poly(sodium 4-styrene sulfonate) (PSS) or chondroitin sulfate C were added to aqueous nanoparticle dispersions. The TEM specimen of PSS-coated nucleotide/lanthanide nanoparticles was prepared as follows. The 5′-AMP/Gd^{3+} nanoparticles collected by centrifugation was redispersed in 0.1 M HEPES buffer (2 mL, containing 1 mg/mL PSS) by ultrasonicaion (BRANSON 2510 (YAMATO)) for 1 min. A drop of obtained dispersion was placed on a carbon-coated copper grid. After 30 s, the droplet was removed by adsorbing to a piece of filter paper and the specimen was dried in vacuum. For DLS measurement, 0.01 mL of this 5′-AMP/Gd^{3+} nanoparticle dispersion was diluted with HEPES buffer solution (0.1 M, 0.99 mL) prior to the measurement. Aqueous dispersions of nanoparticles for luminescence and MRI measurements were prepared as follows. Aqueous dispersions of 5′-NMP/Tb^{3+} (N = A, G, U, and C) nanoparticles for luminescent spectroscopy were prepared by mixing aqueous 5′-NMP disodium salts (10 mM) in 0.1 M HEPES buffer (1 mL, pH 7.4) and aqueous $TbCl_3$ (10 mM, 1 mL) at room temperature. After 2 h, the resultant nanoparticle suspensions were diluted to 0.1 mM with pure water. For MRI measurements, 5′-NMP/Gd^{3+} nanoparticles (N = A and G) were prepared by mixing aqueous 5′-NMP disodium salts (15 mM) in 0.1 M HEPES buffer (1 mL, pH 7.4) and aqueous $GdCl_3$ (10 mM 1 mL) at room temperature. The resultant nanoparticles precipitated were washed with water, and were redispersed in 0.1 M HEPES buffer solution containing PSS (50 μg/mL).

Incorporation of Dyes into Nucleotide/Lanthanide Nanoparticles. To introduce functional materials in nucleotide/lanthanide nanoparticles, dopant materials such as dyes, gold nanoparticles, and proteins were added to aqueous nucleotide solutions prior to the addition of aqueous lanthanide ions. 5′-AMP disodium salt (10 mM) and dyes (0.1 mM) were dissolved in 0.1 M HEPES buffer (1 mL). Dye-doped nucleotide/lanthanide nanoparticles were prepared by mixing these solutions and aqueous $GdCl_3$ (10 mM, 1 mL). The amount of dyes incorporated in nanoparticles was determined by measuring absorption intensity of dyes in the supernatants. Fluorescence quantum yields and lifetimes were measured for dye-doped 5′-AMP/Lu^{3+}nanoparticles cast on quartz and on silicon substrates, respectively. For the CLSM measurement, dye **2**-doped NADH/La^{3+} particles were prepared according to the typical preparing procedure, without ultracentrifugation, washing and redispersing procedure.

Incorporation of Gold Nanoparticls into Nucleotide/Lanthanide Nanoparticles. An aqueous solution of 10 mM $HAuCl_4$ in water (5 mL) was mixed with aqueous 5′-GMP disodium salt (10 mM) in HEPES buffer (0.1 M, 5 mL) with vigorously stirring. Within a minute, the color of solution was changed from yellow to red-purple. In TEM observation (Figure S20, Supporting Information), nanoparticles with diameters of 3−10 nm were observed, indicating that Au^{3+} ions were reduced by HEPES molecules.[18] 5′-GMP molecules are adsorbed on the surface of AuNPs as stabilizer.[19] Then aqueous 5′-GMP-capped AuNPs (50 μL), aqueous 5′-GMP disodium salt (10 mM) in 0.1 M HEPES buffer (50 μL) and aqueous $GdCl_3$ (10 mM, 100 μL) were successively added to an aqueous solution of dextran (10 mg/mL, 2 mL). The obtained precipitates were used for further experiments without the washing process.

Immobilization of Proteins on Nucleotide/Lanthanide Nanoparticles. Immobilization of proteins within nucleotide/lanthanide nanoparticles were performed by mixing aqueous 5′-AMP disodium salt (10 mM) containing 50 μg/mL proteins in 0.1 M HEPES buffer (0.25 mL, pH 7.4) and aqueous $GdCl_3$ (10 mM, 0.25 mL). In the enzymatic activity assay, GOx- and HRP-immobilized 5′-CMP/Eu^{3+} nanoparticles were collected on a Durapore membrane filter (pore size: 0.1 μm, diameter, 2.5 cm, Millipore) by passing 200 μL of nanoparticle dispersion diluted with 0.1 M HEPES buffer (1.8 mL). Then aqueous mixtures of Trinder reagent[25] ([4-aminoantipirine] = 10 mM, and [*N*-ethyl-*N*-(3-sulfopropyl)-3-methoxyaniline] = 10 mM) containing various monosaccharides in 0.1 M HEPES buffer (20 μL, pH 7.4) were placed on nanoparticles immobilized on membrane filters.

***In Vitro* and *in Vivo* Experiments.** HeLa cells were maintained in Dulbecco's modified Eagle's medium containing 10%(v/v) heat-inactivated fetal bovine serum and 1% (v/v) antibiotics (DMEM+FBS) at 37 °C in a humidified atmosphere containing 5% CO_2. For biological studies, chondroitin sulfate C was used as stabilizer because of its biocompatibility. For fluorescent imaging, dye **4**-doped 5′-AMP/Gd^{3+} nanoparticles were prepared. The suspensions of cultured HeLa cells (1×10^5 cells/mL) were added to PLL-coated glass-bottomed dishes (ϕ 10 mm) and cultured in DMEM+FBS for 24 h. After removal of DMEM+FBS, the cells were washed with PBS (3 mL × 3), and were incubated for another 24 h in DMEM+FBS (1 mL) containing dye **4**-doped 5′-AMP/Gd^{3+} nanoparticles. The incubated cells were then observed by fluorescence microscopy. For ICP-MS and fluorescence imaging of tissue samples, dye **4**-doped 5′-AMP/Gd^{3+} nanoparticle dispersed in HEPES buffer was injected into the tail vein of 4-week-old mice (ddY, male) at 28 mg/kg. Further experimental details are described in the Supporting Information.

Acknowledgment. We thank Prof. A. Maruyama (Kyushu University) for the use of CLSM and fluorescence imaging apparatuses. This work was supported by a Grant-in-Aid for Scientific Research A (19205030) from the Japan Society for the Promotion of Science (JSPS), a Grant-in-Aid for the Global COE Program, "Science for Future Molecular Systems" from the Ministry of Education, Culture, Sports, Science and Technology of Japan and by JST, CREST. R.N. acknowledges the JSPS for a JSPS Research Fellowship for Young Scientists.

Supporting Information Available: Additional details for preparation, characterization, and functional evaluation of nucleotide/lanthanide nanoparticles, dye-incorporated nanoparticles, gold nanoparticles-wrapped nanoparticles, and protein-encapsulated nanoparticles. This material is available free of charge via the Internet at http://pubs.acs.org.

JA8058843